arXiv:1408.0693v1 [astro-ph.IM] 4 Aug 2014

Application of algorithms for high precision metrology

M. Gai[1], A. Riva[1], D. Busonero[1], R. Buzzi[1], F. Russo[1]
Istituto Nazionale di Astrofisica - Osservatorio Astrofisico di Torino,
V. Osservatorio 20, 10025 Pino T.se (TO), Italy
gai@oato.inaf.it

ABSTRACT

This paper evaluates the performance of algorithms suitable to process the measurements from two laser beam metrology systems, in particular with reference to the Gaia Basic Angle Monitoring device. The system and signal characteristics are reviewed in order to define the key operating features. The low-level algorithms are defined according to different approaches, starting with a simple, model free method, and progressing to a strategy based on the signal template and variance. The signal model is derived from measured data sets. The performance at micro-arcsec level is verified by simulation in conditions ranging from noiseless to large perturbations.

Subject headings: Astronomical Instrumentation — Data Analysis and Techniques

1. Introduction

High precision astrometry is often supported by metrology, either on ground or in space. An example of the former case is the control of atmospheric disturbances in long baseline interferometry, typically in the near infrared range (Schmid et al. 2012; Robertson et al. 2012), and of the overall instrument geometry (Woillez & Lacour 2013), for narrow to medium angle astrometry. The latter case is mostly aimed at measurement or control of the configuration of a macroscopic instrument to a small fraction of wavelength, for astrometry from intermediate to large angle (Malbet et al. 2012; Unwin et al. 2008a,b; Gai et al. 2012b). The distinguishing aspect of space experiments is that usually the precision goal is referred to a much more compact telescope than ground based instruments, translating the requirements into a much narrower fraction of the diffraction limit; therefore, the constraints on image modeling (Gai et al. 2013) and calibration (Zhai et al. 2011) become correspondingly more challenging.

Metrology usually employs interferometric combination of laser beams to meet the precision goal thanks to the high photon flux. As optoelectronic systems become more and more complex, the metrology signal may be affected by a number of implementation aspects, potentially introducing errors. The data processing algorithms become then a performance factor, as their limitations might compromise part of the potential precision associated to the hardware design.

We address a set of algorithms suited to the relative phase of multiple fringe patterns from two-beam laser interferometry, in particular the low-level, short range automated processing providing the relevant information to higher level diagnostics software and to the scientists evaluating the system response. The current work is focused mainly on the application to the Gaia metrology subsystem, although the concept is quite general and could be applied, in the future, to other high precision astrometry experiments (Gai et al. 2012a).

The Gaia mission (Perryman 2005; de Bruijne 2012) is aimed at global astrometry at the few micro-arcsec (hereafter, μas) level, producing an all-sky catalogue of position, proper motion and parallax, complete to the limiting magnitude $V \simeq 20\,mag$. The Gaia concept relies on self-consistency of the astrometric information of celestial objects throughout operation, factoring out the instrument parameters and their evolution by calibration of the overall data set. The Hipparcos experience suggests that the approach is viable

with respect to detection and modeling of the instrumental parameter secular evolution and long term variations, over time scales longer than a few revolution periods, i.e. above about one day.

Gaia takes advantage of the simultaneous observations of two telescopes mounted on a common high stability torus to measure precisely the relative positions of stars in regions of the sky separated by a wide *basic angle* $BA = 106°.5$. Perturbations to the instrument geometry induce displacements of each telescope *line of sight* (LOS); the common mode displacement of the two telescopes does not affect the measured angular separation between stars, and appears as a disturbance of the overall instrument, with an effect similar to attitude jitter, i.e. a small degradation of image sharpness. However, the differential LOS perturbation appears as a *BA variation* (BAV), which affects directly the astrometric measurement of star separation.

The design specifications are derived from the short term astrometric performance requirements, corresponding to a BA stability $\sigma(BA) \simeq 7\,\mu as$. In order to ensure that the short term stability requirement is actually met throughout operation, a custom on-board metrology system is also integrated in the payload design, the *Basic Angle Monitoring* (BAM) device (Gielesen et al. 2012).

The metrology concept is based on pairs of collimated beams from a laser source, split by a dedicated distribution system in front of the Gaia astronomical telescopes, and following an optical path very close to that of the stellar photons to generate an interferometric pattern on a dedicated section of the focal plane. The rationale is that perturbations to the optical configuration, affecting the position of the stellar images on the focal plane, i.e. the basic ingredient of the astrometric measurement, would affect also the BAM beam path, and therefore the interferogram phase. The match between astronomical and metrology photons is not complete, e.g. because the laser beam hits a much smaller region of the optical system, but it is assumed that the most relevant variations of the telescope geometry will also induce an effect on the interferogram phase, which is monitored, allowing for estimation of astrometric corrections to be applied in the data reduction, if required.

In Sec. 2 we present the main characteristics of the signal, and in Sec. 3 we define accordingly the algorithm concepts. In Sec. 4 we evaluate the performance achieved with a simple implementation of such algorithms; then, in Sec. 5, we discuss the implications of their usage within the Gaia data reduction scheme.

2. Signal characteristics

The BAM design provides a fringe pattern with period comparable with the stellar image size in the high resolution direction, detected by a CCD similar to the science ones used for object detection, astrometry and photometry. The interferogram can be considered as a large set of artificial stars, coherently providing an instrumental phase information. The BAM concept is based on two assumptions:

- small amplitude of the instrument perturbations to be monitored;
- high signal to noise ratio (SNR).

The latter conditions leads to a potential measurement precision corresponding to a small fraction of the interferogram period, thus making the device suitable to fulfill the former requirement.

The actual relationship between the interferogram phase and the telescope pointing direction is unknown, depending on the actual optical configuration, but is it assumed that, in the expected small perturbation regime, they will concide apart an offset, or "zero point". The BA variation, i.e. the variation of the angle between the telescope observing directions, is thus referred to variation of the relative phase between the interferograms. In particular, correlated phase variations are associated to common mode telescope pointing errors, and differential phase variations to more critical BA variations affecting the astrometric measurement.

In the medium to long period, the BA variation measured by the BAM device can be calibrated with respect to its corresponding value on the sky, as deduced by convenient combination of observations, e.g. variation in the angular separation among stars at different epochs. The comparison between BAM measurements and astrometry will therefore provide an assessment of science quality throughout the mission.

The interferogram associated to an ideal BAM, feeding an ideal telescope, is the point spread

function of the unobstructed circular aperture related to the individual laser beams, modulated by fringes with the Young period. Practical implementation introduces deviations from such simple framework, because of optical aberrations due to design, manufacturing and alignment in the metrology distribution system and in the telescope. Also, the laser beam intensity is not uniform over its cross section, but it is expected to be described e.g. by a truncated Gaussian.

This still generates a useful signal (Riva et al. 2012) with high contrast fringes within a more complex diffraction envelope. The fringe period is basically preserved, but the phase modulation bears contributions from the real system. Also, the envelope has generally larger size, and significant shape variation, with respect to the ideal case. However, it is expected that the crucial information of BA variation is still encoded in the mutual relationship between interferograms. In particular, the small BA variations expected during operation will introduce interferogram displacements on the μas scale, with amplitude much smaller than the fringe period.

The BAM device, by design, generates an interferogram for each telescope, imaged in different positions of a common dedicated CCD. Each signal is affected by its own photon shot noise, background (depending on the current pointing position), and comparable readout noise. Photon noise is expected to be the main contribution, since the laser source intensity is tuned in order to use most of the detector dynamic range.

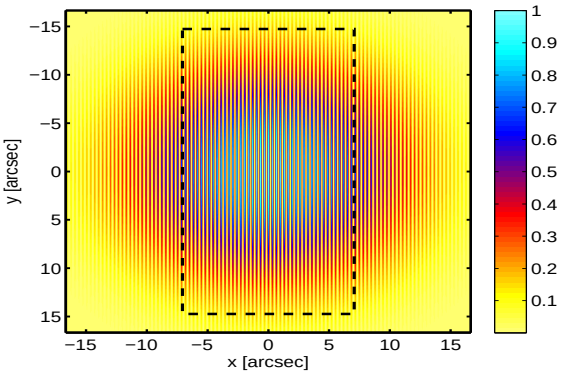

Fig. 1.— Gaia BAM interferogram; dashed rectangle: readout area

The BAM is based on a geometry similar to that of Young's interference experiment, in which the two slits are replaced by small beams with diameter $D = 9\,mm$, separated by a baseline $B = 0.54\,m$, generating on the focal plane a modulated signal, i.e. an interferogram, with $\sim 2.44B/D = 146$ fringes, limited by the diffraction envelope of the individual aperture. The two telescopes are fed by separate beam pairs, generating similar interferometric spots on the detector; the fringe period is $\lambda/B = 325\,mas$, corresponding to $55\,\mu m$, i.e. 5.5 pixels. The interferogram from each telescope is repeatedly measured, at a rate of an image every $\sim 20\,s$.

Hereafter, we will refer to the beam pair monitoring one telescope, to the related optical system, and to the corresponding detected signal, as a "BAM channel". Only a limited region of interest over the central lobe of diffraction is actually acquired, for each BAM channel, as shown by the dashed rectangle in Fig. 1. The interferogram is integrated across the fringes after readout, in order to achieve a more easily tractable one-dimensional signal, shown in Fig. 2. Since the fringe patterns are mostly aligned to the CCD array, to within $1^\circ.5$, only a marginal smearing is introduced.

3. Algorithm definition

The laser source is monochromatic, but the interferometric signal, due to the limited beam diameter and associated fringe envelope size, has a spatial frequency distribution spread over the ap-

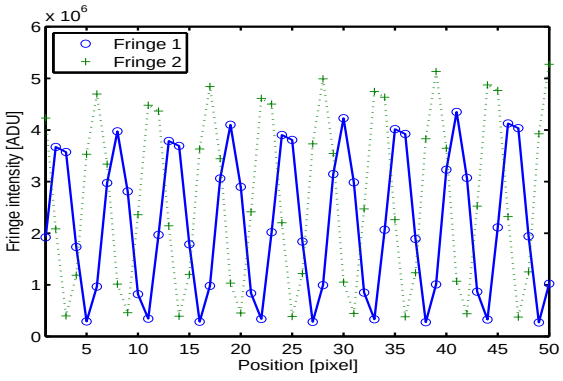

Fig. 2.— Section of two one-dimensional fringe patterns, integrated across fringe

proximate range $\left[\frac{\lambda}{B+D}, \frac{\lambda}{B-D}\right]$. A detailed mathematical description of the fringe pattern is not easily formulated except in the simplest geometric cases, due to optical aberrations.

However, most phase estimation algorithms are based either on a template, or on assumptions on the mathematical characteristics of the signal, i.e. they are *model dependent*. Given the BAM readout frequency and high SNR, it is possible to define a numerical *signal template*, as well as its empirical variance, both deduced from a convenient set of measured data, rather than analytical formulation of a signal model whose parameters have to be estimated e.g. by best fit to the measurements.

It is possible to define algorithms aimed at providing a phase estimate for each interferogram, related to the average LOS position of the individual telescope, from which the BAV is simply deduced by difference of the phase values at each time. We focus on a set of simple concepts leading to convenient algorithm implementation, and evaluate their main impact on the measurements.

We also address a *model independent* measurement concept, providing a direct estimate of the BAV as phase difference between the fringe patterns, without individual phase computation.

A model dependent approach is expected to be, in principle, more precise, because the expected characteristics of the signal are taken into account. However, this requires that additional information is available to define at least the signal template and variance, as in Sec. 3.1. Hereafter we expand on some of the possible approaches, which will then be tested on simulated data.

3.1. Template definition from the data

From a sufficient number N of measurement of the interferometric signals S_1, S_2 related to each telescope, it is possible to define the sample approximations T_1, T_2 of the corresponding templates, or noise free reference functions, from the signal averaged over the data set:

$$T_{1,2}(x_k) = \frac{1}{N}\sum_{n=1}^{N} S_{1,2}(x_k; t_n) \ . \qquad (1)$$

The dependence on the pixel position x_k and on the current exposure time t_n has been shown explicitly, but it will be omitted below where not necessary for the sake of simplicity.

We define in a similar way the empirical variance V_1, V_2 of each interferogram pixel as

$$V_{1,2}(x_k) = \frac{1}{N-1}\sum_{n=1}^{N} \left[S_{1,2} - T_{1,2}\right]^2 \ . \qquad (2)$$

This approach is based on the assumption that the measurement conditions are stationary, so that the average can be considered as a reasonable approximation of the template.

The phase noise on the fringes is assumed to be much smaller than the fringe period, by a factor of $\sim 10^{-5}$, in normal conditions. However, phase noise will induce errors on the template and variance estimate, in addition to the amplitude fluctuations due to photon noise. It can be shown that photon noise, in the expected conditions, is dominant; thus, the small fringe displacement among subsequent instances does not introduce a significant blurring of the mean fringe, which can be considered a reasonable approximation to the desired signal template.

In the numerical experiments below, the template is built by averaging over $1,000$ frames, so that the expected reduction of individual measurement noise is of order of $\sqrt{1000} \simeq 31$.

The data set also provides an estimate of the signal dispersion through the sample variance, so that subsequent measurements can then be checked for consistency with the template and the initial data (e.g. in terms of confidence levels). For each BAM channel, a specific template is defined by averaging the corresponding data set from a suitable measurement sequence.

3.2. Model free fringe location: Mutual Correlation (MC)

The signals from the two BAM channels are not exactly sinusoidal, but they have a very narrow spectrum, resulting in a significant modulation at the same nominal spatial frequency. Their envelopes are not equally shaped, but over the readout region their amplitude is quite high.

The signal similarity leads to the possibility of processing them with a simple approach based on the correlation technique. The two quasi sinusoidal signals will have a maximum correlation value for a given displacement with respect to each other, which in the example shown in Fig. 2 is of

order of two pixels. A perturbation to whichever telescope, inducing a phase variation on the corresponding interferogram, will modify accordingly the position of the signal correlation maximum. Therefore, this algorithm defines a linear variable strictly related to the relative position of the interferograms, and as a consequence of the basic angle variation between telescope lines of sight.

We adopt the estimate of this relative interferogram phase as an operational definition of the BA estimate, in order to monitor its variation around an irrelevant zero point to be calibrated on the sky from science data. This approach, by construction, gives a position estimate modulo the fringe period, which is not an "absolute" datum.

The relative displacement of the two fringe patterns can be estimated directly by computation of the maximum correlation position between them, e.g. from parabolic fit of the three correlation values achieved for lag zero and ± 1 pixel. This approach completely avoids the issue of template definition; broadly speaking, the interferogram from each channel acts as a template for the other. In practice, the method does not need that the two signals are very similar to each other (which would improve on the correlation value), but only that their shape remains approximately stable over the time frame required for calibration on the sky through the science data.

In more detail, the two signals are arrays of 500 values; given their offset of about two pixels, shown in Fig. 2, they are roughly "aligned" by removing the first value on the former and the last one on the latter, i.e. reducing the data to $K = 499$ values. The offset is due to the simulated placement of readout windows; it is constant over the simulation, due to the small phase noise.

The lag zero signal is then selected as the central part of the array with index $k = 2, \ldots, K-1$, i.e. excluding the end values. The lag ± 1 signals include respectively either of the end values, discarding the opposite ending value, i.e. with indices $k = 1, \ldots, K-2$ and $k = 3, \ldots, K$. The correlation is then computed over $K - 1 = 498$ values. This windowing approach sacrifices a small part of the signal, but it avoids data interpolation, or extrapolation at each end of the arrays. Processing is fast, as only array indexing is used.

The mismatch between signals from each BAM channel suggests that the noise performance of this algorithm may not be optimal, but its advantages are the simplicity and robustness, so that it is applicable also in a context of limited knowledge of the instrument parameters, e.g. at the beginning of operation or after unexpected events inducing large perturbations. It also provides a simple sanity check for other algorithms.

3.3. Model dependent fringe location: Correlation with Template (CT)

In the expected operating conditions, the interferometric signal is quite stable, therefore we assume that it is possible to apply the approach of Sec. 3.1 to define its model (or template) by averaging the measurements according to Eq. 1. As far as only small perturbations are present, the individual signal instances will be consistent with such signal template, apart from fluctuations in amplitude (e.g. from photon noise) and phase (related to the BA variation).

For any fringe pattern instance, we compute the correlation with the template, in its nominal position, and with ± 1 pixel offset. The indexing of Sec. 3.2 is used for definition of the lag zero and ± 1 signals. Also, parabolic fit of the correlation values provides the "exact" location of the current interferogram with respect to its template. *We adopt this parameter as an estimate of the relative LOS position, independently for each BAM channel.* The difference between LOS values is considered the operational definition of the BA, so that its variation can be used for monitoring.

In stable conditions, each LOS is expected to fluctuate around zero, since each signal instance is close to its template within the noise; similarly, the BA estimate is expected to be centered in zero.

3.4. Model dependent fringe location: Maximum Likelihood estimator (ML)

Correlation is a robust and proven technique, but it is known to provide sometimes less than optimal noise performance. We define an estimator derived in the maximum likelihood framework, which also requires knowledge of the current noise statistics, in particular the signal variance, estimated on the data as from Eq. 2.

Given two similar functions, hereafter labeled "signal" S and "template" T, the maximum like-

lyhood approach may be used to identify the best matching position, minimizing a functional inspired to the classical χ^2 and defined as

$$\chi^2 = \sum_{k=1}^{K} \frac{[S_k - T(x_k - \tau)]^2}{\sigma_k^2}, \qquad (3)$$

where the dependence on the coordinates has been shown explicitly only for the template. The matching position has true value τ_0, and its estimate τ is derived from the measured data. The derivation follows that in Gai et al. (1998), in which the signal $S_k = S(x_k)$, measured over the K pixel positions x_k, was considered as equal to the template T apart an unbiased measurement error and a shift in the reference position, therein labelled "photo-centre". It may be noted that, in case of usage of different functions, e.g. a template not matching the signal, or an evolving signal shape (non stationary conditions), the signal discrepancy

$$h_k = S_k - T_k \qquad (4)$$

is no longer just due to noise, so that it cannot be expected in general to be uncorrelated and to have zero mean.

The photo-centre estimate must be a stationary point of the χ^2 in Eq. 3, i.e. a solution of the equation

$$\sum_k \frac{[S_k - T_k(\tau_0)] \cdot T'_k(\tau_0)}{\sigma_k^2(\tau_0)} = 0. \qquad (5)$$

Therefore, assuming small errors ($\tau \approx \tau_0$), the square bracket can be simplified, taking advantage of Taylor's expansion of the template in the current approximate position, to provide

$$\tau - \tau_0 = -\frac{\sum_k \frac{[S_k - T_k(\tau)] \cdot T'_k(\tau)}{\sigma_k^2(\tau)}}{\sum_k \frac{[T'_k(\tau)]^2}{\sigma_k^2(\tau)}}. \qquad (6)$$

The solution is unbiased, i.e. $\langle \tau - \tau_0 \rangle \equiv 0$, and has variance equal to

$$\left\langle (\tau - \tau_0)^2 \right\rangle = \left[\sum_k \frac{[T'_k(\tau)]^2}{\sigma_k^2(\tau)} \right]^{-1}. \qquad (7)$$

It may be noted that at increasing values of location error, due e.g. to lower SNR, the validity of the above expressions degrades progressively. *The above Eq. 6 is adopted as operational definition of the ML estimate of LOS, for each BAM channel, and the BA is defined as the LOS difference.*

3.5. Residual diagnostics

In order to assess the consistency of individual interferogram S_k with the current estimate of signal template T and of its variance V, from Eqs. 1 and 2, we define a quantity related to the reduced χ^2 concept according to Eq. 3:

$$\chi_R^2 = \frac{1}{K-1} \sum_{k=1}^{K} \frac{[S_k - T(x_k - \tau)]^2}{\sigma_k^2}. \qquad (8)$$

When all residuals are comparable with the expected noise, corresponding to the signal variance, the reduced χ^2 is expected to be of order of unity. The normalisation factor $K-1$ is used under the assumption that no model parameter is derived from the current measurement, apart an overall photometric level estimate. The issue of defining the actual number of degrees of freedom is quite sensitive, in general, and may require some care in practical implementation.

However, we may expect that the value of χ_R^2 as defined in Eq. 8 might at least help in identifying significant perturbations, when it becomes significantly larger than unity.

4. Simulation

The algorithm performance is evaluated, first of all, in terms of noise sensitivity with respect to signal amplitude, and of linearity with respect to signal phase; then, on externally generated data, with respect to random noise and systematic error performance. The processing is performed on a desktop PC, endowed with an Intel Xeon 3.33 GHz CPU and 8 GB RAM, using the Windows 7 (64 bit) operating system, and the Matlab package.

4.1. Performance as a function of amplitude noise

The phase noise performance is simulated for the three algorithms defined above, using signal profiles considered as realistic for an optical configuration affected by a plausible amount of manufacturing, mounting and alignment errors.

Over a range of intensity corresponding to increasing SNR, from few hundreds to about one million, we estimate the theoretical location precision for the ML algorithm according to Eq. 7. For

each algorithm, we generate a noisy signal sample of $N = 10,000$ instances, corresponding to constant interferogram phase and random amplitude fluctuations related to the photon noise level associated to the current intensity level. The fringe position, or the corresponding interferogram separation, is estimated according to a simple implementation of each algorithm (MC, CT, ML). The corresponding BA noise due to amplitude fluctuations is then evaluated as the RMS dispersion over the sample. The result is shown in Fig. 3. Over most of the SNR range, the trend is basically photon limited, as evidenced by the constant slope in logarithmic units.

The noise decreases with increasing SNR, as expected, and the algorithm performance difference cannot be easily distinguished on this scale. In order to ease the comparison of algorithm results, the relative precision is shown, referred to the estimated precision from Eq. 7, which can be considered as a conservative estimate of the limiting performance, providing a good match with the Maximum Likelihood location estimator defined in the same framework. The result is shown in Fig. 4.

In the high SNR regime, the noise performance of both correlation methods is comparable, and about 10% (CT) and 12.5% (MC) worse than the limiting error defined in the Maximum Likelihood framework. The fluctuations of the relative performance are compatible with the statistics related to the sample size, i.e. of order of 1%.

4.2. Linearity performance

The algorithm linearity is evaluated in a noiseless case by simulation, injecting a known LOS displacement on the input signals and verifying the LOS estimate in output (for CT and ML). For the MC algorithm, the BAV estimate is averaged for input displacements applied to either LOS1 or LOS2 (both giving quite similar, but not exactly equal, results). The test range is $\pm 1\,mas$, i.e. quite large with respect to the small perturbations expected in the normal operating regime. A linearity correction was required for both CT and MC. The input/output discrepancy of ML, and the corresponding residual discrepancy after linearity correction for CT and MC, are shown in Fig. 5.

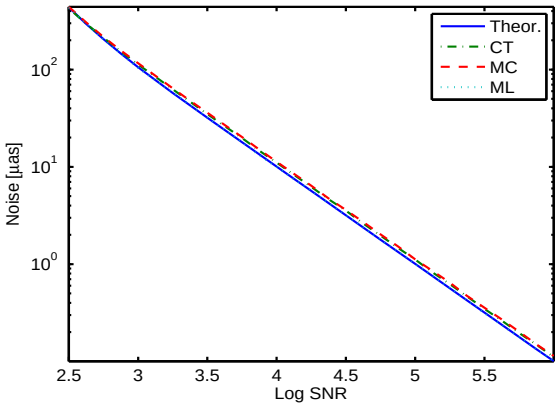

Fig. 3.— Algorithm precision as a function of SNR

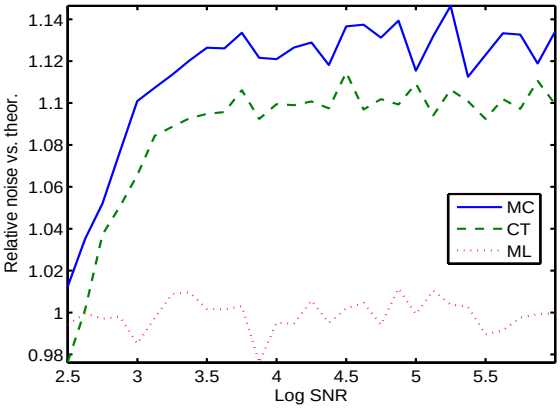

Fig. 4.— Noise with respect to the ML case

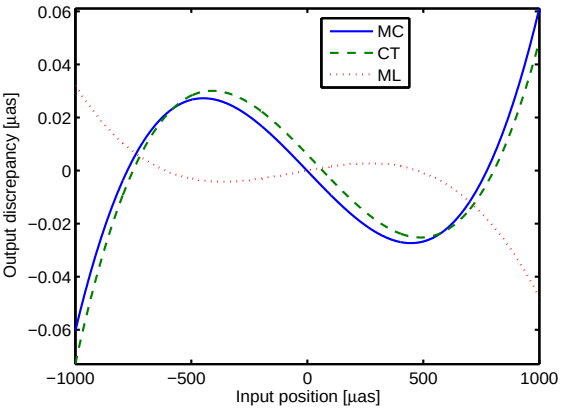

Fig. 5.— Input/output discrepancy for ML, CT and MC

The linearity of all algorithms, after correction in the case of MC and CT, is quite good, providing a residual discrepancy of a few 0.01 μas over the $\pm 1000\,\mu as$ range considered.

4.3. Performance of the algorithms on externally simulated data

Two data sets including a number of realistic effects have been generated by the Coordination Unit 2 (CU2) of the Gaia Data Processing and Analysis Consortium (DPAC), on the supercomputer Mare Nostrum at the Barcelona Supercomputing Center (Centro Nacional de Supercomputación), including contributions from different real world sources. They are processed according to the algorithms in Sec. 3. The data sets include respectively 5,181 and 3,638 interferogram pairs representing sequences of BAM exposures.

4.3.1. Overall features of the data set 1

The signal to noise ratio of this set of fringe pattern pairs is extremely high, of order of 6×10^5 and 10^6 respectively for the whole LOS 1 and LOS 2 signals. From Sec. 4.1, this corresponds to an astrometric noise level of order of 0.2 μas and 0.1 μas, respectively.

At an early analysis, a discontinuity in the data set was evidenced, as can be seen in Fig. 6, showing the average intensity over each interferogram (i.e. the mean level of the fringe pattern). This intensity variation might correspond e.g. to a variation of the laser source intensity, although the amplitude of the variation ($\sim 20\%$) and its suddenness may not be expected as a realistic common event. However, it is interesting to check the robustness of our diagnostics and measurement algorithms against such variations.

Given the relative stability of the signal level on each side of the discontinuity, we compute the signal template and variance separately for each subset, according to Eqs. 1 and 2; they are labeled respectively "Pre" and "Post", with reference to the discontinuity. According to Sec. 3.5, we evaluate the reduced χ^2 for each interferogram using both templates. The results are shown in Fig. 7.

We remark that the large signal amplitude variation in Fig. 6 is evidenced also by a huge χ^2 variation, by about seven orders of magnitude, when processing the data on either side of the discontinuity with the mismatched template. The χ^2 increase is consistent with the intensity variation and the SNR level: the signal change is order of 10^4 times larger than its variance. Besides, using matched data and templates, i.e. "Pre" template with "Pre" data and "Post" template with "Post" data, the reduced χ^2 value remains of order of unity, as shown in Fig. 7.

4.3.2. LOS and BAV of the data set 1

The LOS evolution over the data set 1 are shown in Fig. 8, estimated using the CT algorithm. The linearity correction from Sec. 4.2 is applied. In Fig. 9 the LOS estimate from the ML algorithm is shown. A crude background subtraction is applied, by removing the fringe mean value. The zero points have been set according to display convenience; also, each display point replaces 10 initial points with their average, also reducing the noise, in order to improve on plot readability.

The ML result is quite similar to that from CT for both LOS 1 and LOS 2. The two algorithms appear therefore to be quite consistent with each other. The signal discontinuity appears to induce a marginal effect on both LOS 1 and LOS 2, corresponding to an offset of a few 0.1 μas. Both LOSs feature an approximately sinusoidal behaviour, with different phase, and period corresponding to the satellite revolution (about six hours). The oscillations are referred to simulation of the thermo-elastic evolution of the instrument during the spin, i.e. a physical phenomenon; the two telescopes are mounted in different po-

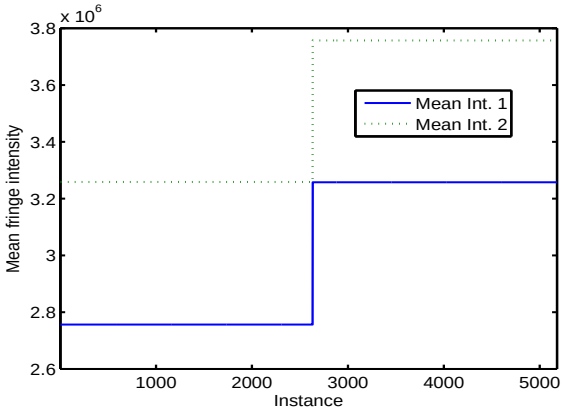

Fig. 6.— Mean fringe intensity, data set 1

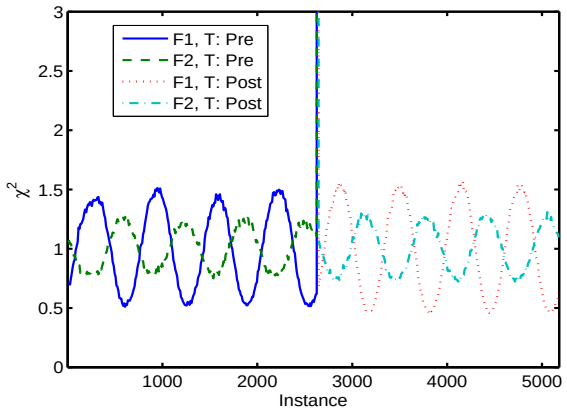

Fig. 7.— Reduced χ^2, zoom on unity; data set 1

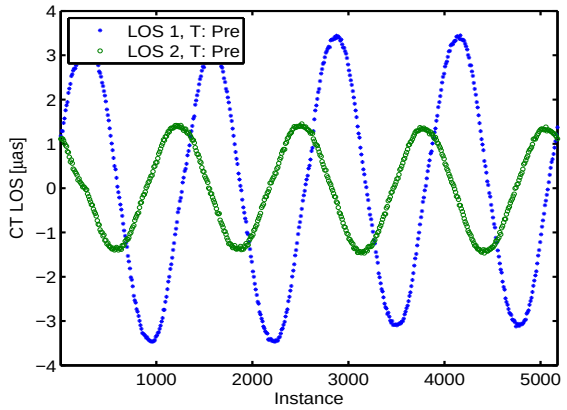

Fig. 8.— LOS estimate by CT; data set 1

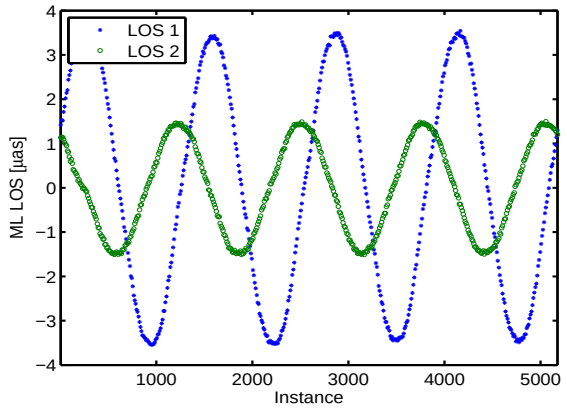

Fig. 9.— LOS estimate by ML; data set 1

sitions and therefore respond independently to a given external perturbation (e.g. residual effects of Sun irradiation). Besides, the LOS and BAV "jump" is due to the change in the signal profile between either side of the discontinuity, filtered by the truncation due to readout windowing and the algorithm response.

The sequence of BAV estimates from each algorithm is shown in Fig. 10, also including the nominal BAV values used in input to the simulation (solid line). It may be noted that all algorithms reproduce a large part of the input BA oscillations, to a few 0.1 μas.

The BAV discrepancy from the input value is shown in Fig. 11 for each algorithm. The effect of signal discontinuity is a small BAV "jump" (by a few 0.1 μas) on CT and MC estimates (circles and crosses, respectively), and hardly perceivable ($\sim 0.1\,\mu as$) on the ML results (triangles).

The mean and RMS discrepancy of the results from each algorithm with respect to the "true" input BAV, and of the result discrepancy between algorithms, are listed in Table 1 separately for the two region. The input/output BAV discrepancy is the algorithm error (a few 0.1 μas for MC and CT, a few 0.01 μas for ML), whereas the output difference (a few 0.1 μas) is related to the mutual algorithm consistency. The RMS values can be considered as the random noise of the measurement, whereas the offsets represent a systematic difference.

The noise is of order of 0.1 μas, as expected, within each data region ("Pre" or "Post"); the av-

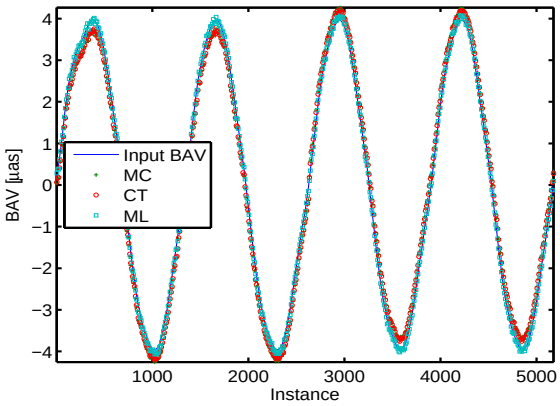

Fig. 10.— Input and estimated BAV; data set 1

erage value is quite close to zero for ML, evidencing a very small systematic error, consistent with the very small "jump" (Fig. 11). The results from the different algorithms are consistent to within a few $0.1\,\mu as$.

The MC and CT results are grouped along straight lines separated by a vertical offset, corresponding to a "jump" (associated to the signal discontinuity) of $\sim 0.5\,\mu as$, significantly larger than the intrinsic dispersion in either "Pre" or "Post" region.

The algorithm linearity can be verified by direct comparison of input and output values; the ideal case of perfect matching between input and output would correspond to zero discrepancy. The BAV discrepancy is shown in Fig. 12 for all three algorithms. Their response is quite linear, since the slope of the output discrepancy vs. input BAV is very small; the offsets are again due to the signal discontinuity. The analysis of linear correlation between input and output provides a correlation coefficient in all cases above 99.9%, and a slope very close to unity, for all algorithms.

4.3.3. Results on data set 2

The SNR of this data set is still very high with respect to usual astronomical data, but significantly lower than the previous case, of order of 5×10^4 for both LOS 1 and LOS 2 signals, corresponding to the nominal BAM operation level. From the results of Sec. 4.1, this corresponds to an expected astrometric noise level of order of $1\,\mu as$.

The simulation results evidence a noise level of $\sim 1.4\,\mu as$, consistent with the expectations. The algorithm behaviour with respect to signal perturbations, including intensity increase by 14% for channel 1, and 12% for channel 2, is again limited to a BAV "jump" of about $1\,\mu as$. The results from MC, CT and ML remain quite consistent with each other. Also, the signal variation is clearly evidenced by the reduced χ^2.

5. Discussion

The performance of low-level algorithm on BAV noise and linearity has been verified on different data sets at the μas level or better, consistently with the SNR limit. In spite of its simplicity, the model free approach (MC) achieves noise performance within a few percent of the template based CT and within $\sim$ 12.5% of the ML limit. MC results are also quite consistent with those from CT, but with lower sensitivity to measurement "jumps" induced by some signal changes. The ML approach takes full advantage of the available information, thus resulting in best noise performance and very little sensitivity to the perturbations simulated in the data sets used.

The availability of different algorithms with comparable sensitivity, and somewhat different response to signal disturbances, may help in detecting perturbations throughout operation by evidencing their effects, and minimising their impact on the science measurements by appropriate corrections introduced in the data reduction. The low-level algorithms do not perform any interpretation of the signal variation simulated in data set

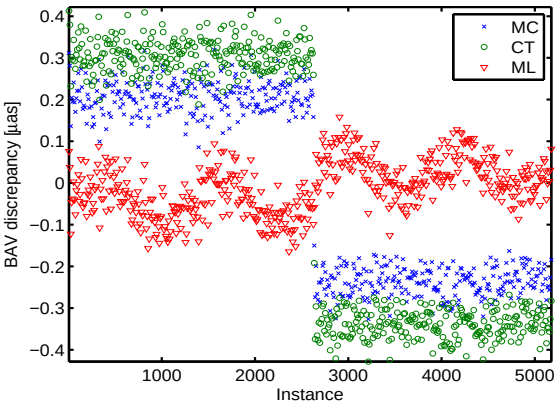

Fig. 11.— Input/output discrepancies; data set 1

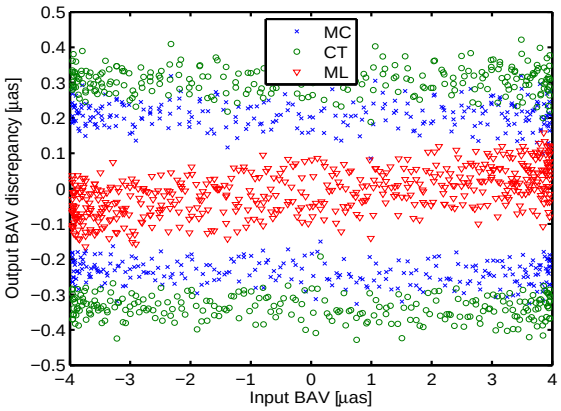

Fig. 12.— BAV discrepancy vs. input BAV

1, in terms of estimation of relevant system parameter change, however they provide a clear diagnostics of its occurrence through the χ^2, and the BAV estimate error is retained within the specifications.

The reduced χ^2 evidences oscillations around unity value on the data set 1 (Fig. 7), even using the matching template and variance for each data subset. This is assumed to be related to the extremely high SNR, and correspondingly very low measurement noise. In such circumstances, the simple procedure used to build the signal template and variance seems to be insufficient, e.g. because the input phase variation induces signal variations not negligible with respect to those associated to photon noise. The fluctuations on ML estimates (Fig. 11), in phase with the BAV, appear to be consistent with this scenario. Such oscillations are no longer present in the reduced χ^2 and BAV computed on data set 2.

The current simple approach appears to be adequate to the Gaia mission requirements, even in spite of the large simulated signal variations, resulting in systematic errors compatible with the micro-arcsec noise level associated with the SNR range expected for the Gaia BAM operation. It may be noted that, with the Gaia pixel size $\sim 60\,mas$, the best precision case of data set 1, of order of $0.1\,\mu as$, corresponds to a few micro-pixels, thus matching well the simulations and experimental results in Zhai et al. (2011).

The minimisation of signal model error, according to Sec. 3.1, requires large amounts of data to average out the noise fluctuations. Besides, this may reduce the sensitivity to disturbances acting on a time scale shorter than the period of data accumulation. A suitable trade-off must therefore be defined.

6. Conclusions

We investigate algorithms aimed at low-level processing of metrology signals from two laser beam, high dilution, imaging metrology systems, with particular reference to the Gaia BAM device. The methods range from a model free approach based on mutual correlation (MC), to others using progressively more detailed information, including the signal template (CT), and the signal variance (ML).

The numerical model of the signal is derived by computing the average fringe pattern and its variance over a convenient data set, which may be easily verified for self-consistency, and has minimal dependence on external parameters: mainly pixel size and optical scale to convert linear results (fractions of pixel) into angular values.

The performance is verified at or below the μas level by simulation on data sets generated either in house, or by independent groups, ranging from the noiseless case to comparably large perturbations. The model free approach still provides quite appealing performance, while the maximum likelihood method features lowest noise and sensitivity to disturbances. Some signal disturbances, including profile variation and up to 20% intensity variation, induce discontinuities in the measured positions of order of $1\,\mu as$, within the design specifications. The signal variation is anyway clearly identified by χ^2 diagnostics.

The performance of all low-level algorithms appears therefore to be of interest for application to the data reduction of the Gaia Basic Angle Monitoring device, and potentially to future high precision astrometry experiments.

The activity described in this paper is partially supported by the contract ASI I/058/10/0. We acknowledge the contribution of the Coordination Unit 2 (CU2) of the Gaia Data Processing and Analysis Consortium (DPAC) for the generation of the BAM data used for some of our tests. Such data have been simulated on the supercomputer Mare Nostrum at Barcelona Supercomputing Center (Centro Nacional de Supercomputación).

REFERENCES

de Bruijne J. H. J., 2012, Ap&SS, online pubblication

Gai M., Casertano S., Carollo D., Lattanzi M. G., 1998, PASP, 110, 848

Gai, M., Busonero, D., & Riva, A. 2012, Proc. SPIE, 8442, 84421O

Gai, M., Vecchiato, A., Ligori, S., Sozzetti, A., & Lattanzi, M. G. 2012, Exp. Astr., 34, 165

Gai, M., Busonero, D., & Cancelliere, R. 2013, PASP, 125, 444

Gielesen, W., de Bruijn, D., van den Dool, T., et al. 2012, Proc. SPIE, 8442, 84421R

Malbet, F. et al., 2012, Exp. Astr., 34(2), 385

Perryman M. A. C., 2005, in P. K. Seidelmann & A. K. B. Monet ed., Vol. 338 of ASP Conf. Series, 3

Riva, A., Gai, M., & Lattanzi, M. G. 2012, Proc. SPIE, 8444, 84445A

Robertson, J. G., Ireland, M. J., Tango, W. J., et al. 2012, Proc. SPIE, 8445, 84450N

Schmid, C., Abuter, R., Merand, A., et al. 2012, Proc. SPIE, 8445, 84450F

Unwin, S. C., Shao, M., & Edberg, S. J. 2008, Proc. SPIE, 7013, 70132L

Unwin, S. C., Shao, M., Tanner, A. M., et al. 2008, PASP, 120, 38

Woillez, J.; Lacour, S., 2013, ApJ, 764(1), 109

Zhai, C., Shao, M., Goullioud, R., & Nemati, B. 2011, Royal Soc. of London Proc. Series A, 467, 3550

This 2-column preprint was prepared with the AAS LaTeX macros v5.2.

Table 1: Algorithm accuracy and consistency before and after the signal discontinuity; data set 1

	CT error $[\mu as]$	MC error $[\mu as]$	ML error $[\mu as]$	CT - MC $[\mu as]$	CT - ML $[\mu as]$	MC - ML $[\mu as]$
Mean Pre	-0.231	-0.272	-0.046	0.041	-0.185	-0.227
RMS Pre	0.127	0.127	0.138	0.012	0.059	0.055
Mean Post	0.218	0.260	0.026	-0.043	0.191	0.234
RMS Post	0.107	0.106	0.118	0.012	0.059	0.055